First passively-illuminated, high-resolution polarimetric images of exhaust plumes from flying rockets

David W. Tyler[a,b], Adam M. Phenis[c], Alan B. Tietjen[d], Miguel Virgen[e]
Jason D. Mudge[e], John S. Stryjewski[d], Jeff A. Dank[e]

[a]Modeling, Simulation, & Information Sciences Dept., Advanced Technology Center, Lockheed Martin Space Systems Co., 1111 Lockheed Martin Way, O/ABCS, B/153, Sunnyvale, CA 94089
[b]College of Optical Sciences, The University of Arizona, 1630 E. University Blvd., Tucson, AZ 85721
[c]AOptix Technologies, 695 Campbell Technology Pkwy., Campbell, CA 95008
[d] Innovative Science & Technology Experimental Facility, ISTEF-CSC, Bldg. N6-2247, Tel-4 Road, Kennedy Space Center, FL 32899
[e]Optics & Electro-Optics Dept, Advanced Technology Center, Lockheed Martin Space Systems Co., 3251 Hanover St., O/ABDS, B/202, Palo Alto, CA 94304

ABSTRACT

We present the first high spatial resolution, passively-illuminated polarimetric images of boosting rocket exhaust plumes. The images shown here show significant linear and circular polarization, and the ability to resolve the polarization signals into images allows us to make some preliminary arguments as to their origins. Our observations are consistent with polarization caused by Rayleigh and Mie scattering (linear) and interaction with plume plasma-generated magnetic fields (circular). We also present nearly simultaneous, two-color, narrow-band (633 ± 5 and 750 ± 5 nm) exhaust plume images, where significant structural differences are observed in the plumes despite a relative small difference in the two wavelengths.

Keywords: Rocket exhaust plumes; imaging polarimetry

1. INTRODUCTION

Rocket engine plumes are rich in signature phenomenology, such as continuum and narrow band spectral radiance, laser and radar scattering cross-sections, acoustic spectra, and polarization phenomena. The latter can be revealed by both passive Stokes polarimetry and active Mueller polarimetry measurements.

Techniques exist for both spectroscopy and polarimetry that allow signatures to be mapped to particular field angles in recorded image data. Applied to rocket plumes, such techniques provide a further enrichment to signature phenomenology by allowing similar signatures to be differentiated based on their spatial distribution. Simultaneous, "snap-shot" polarization[1] and spectral imaging[2] techniques have the advantage over sequential-imaging and scanning techniques for observation of boosting vehicles, because aspect angle, atmospheric path, vehicle velocity, and the aerodynamic and plume flow fields are all changing rapidly.

To unlock the complex physics behind these signatures, a number of rocket exhaust plume signature codes have been developed. These codes predict the infrared spectral distribution of steady-state plume intensity with fairly high accuracy; however, the codes tend to be progressively less accurate as one examines the simulated plume on finer and finer spatial scales. This is because the details of the associated fluid dynamics start to become relatively more important at smaller scales, and incorporating the required computations would make existing

Further author information (Send correspondence to DWT): E-mail: david.tyler@lmco.com, Telephone: 623.826.1677

codes fairly cumbersome and time-consuming to use. Further, the availability of codes to model signatures other than steady-state IR spectra, including polarization, is almost non-existent.

As a consequence, it's reasonable to look to imaging spectrometry, multi-spectral imaging, and polarimetry of rocket plumes for scaling laws around which to build fast, first-order plume models and anchor more comprehensive, *ab initio* simulations. Much of the experimental work in this area has been carried out at the Innovative Science & Technology Experimental Facility (ISTEF) in Florida. The ISTEF site is near Cape Canaveral and includes precision-tracking telescope mounts. ISTEF observations have been used to validate numerical simulations of Atlas engine plume radiometry[3–8] and quantify laser backscatter and polarimetry phenomena[9–12] associated with solid- and liquid-fuel rocket plumes. These efforts include the first two-band focal-plane array (3-5 μm and 8-12 μm) images of a rocket exhaust plume (in this case, an Atlas 5).[13] ISTEF has conducted a long campaign of multi-spectral observations in UV, visible, NIR, MWIR, and LWIR for Navy SPAWAR.

Motivated by a desire to both acquire model-validating data and test innovative new sensor technology in a demanding environment, Lockheed Martin's Advanced Technology Center (ATC) recently collaborated with CSC at ISTEF to conduct imaging polarimetry and narrow-band, multi-spectral imaging of rocket exhaust plumes. To our knowledge, the results presented here are the first high-resolution, passive (no laser illumination) polarization images of rocket engine plumes. We acknowledge the work of Beiting, et al.,[14] and their low-resolution, passive imaging polarimetry of high-altitude Titan IV plumes to establish rocket engine contrail dispersion characteristics. In this paper, we describe our experiments and present preliminary linear and circular polarization images. Section 2 is a description of the observations, including the launch events and the instrumentation. We present image results in Sec. 3 and our conclusions regarding this preliminary analysis in Sec. 4.

2. OBSERVATIONS

As described in more detail below, we observed the launches of an Atlas 5, a Delta 2, and a Space Shuttle. The observations were carried out by mounting the ATC's Simultaneous Stokes Imaging Polarimeter (SSIP) to the tracking mount for ISTEF's 20″ Graz telescope. The Graz mount sits in a dome with a floor 30 ft off the ground. The elevation and the ability to point horizontally means instrumentation on this mount has line-of-sight visibility of Delta rockets while they are sitting on the launch pad. The mount also has a very nearly unobstructed view of the Atlas launch pad, and the Space Shuttle is visibly within seconds of liftoff, as well. Our observing plan was to start recording data with the camera FOV centered on the engine bells, when the possibility of the plume saturating the camera was strongest, then move the FOV gradually down the plume as the rockets ascend. This plan was substantially more difficult to implement with the Delta 2 due to the proximity of the Delta pads to ISTEF, the Delta's acceleration immediately after liftoff, and the fact that shortly after liftoff, the Delta began a turn almost directly away from the site.

Optimal SSIP exposure times for the Atlas launch were estimated by constructing a transmission model of the instrument and using Atlas 3 radiance data found in Barton, et al.[4] The observations reported in this paper were of an Atlas 3, with the same main engine as the Atlas 5. The Atlas 3 was also launched from the same pad as the Atlas 5 we observed, so the variability in brightness was reduced to the solid rocket booster type and configuration as well as any difference in trajectory. To account for a range of possible brightness, data was recorded at progressively increasing exposure times, starting with 10 ms. Six images were recorded at 10-60 ms exposure times; this process was repeated over and over during the launch, recognizing that some images would be saturated and some would have unusably low signal-to-noise. Lacking radiometric data for the Delta and shuttle launch vehicles, and with those launch pads in different locations than the Atlas pads, we simply assumed the set of exposure times that worked with the Atlas would produce reasonable results for the other two launches.

2.1. Instrumentation and data reduction

The ATC SSIP sensor was described by Phenis, et al.[1] The SSIP is a division-of-aperture imaging polarimeter (DoAP). A more advanced instrument, the "Gen II" SSIP, is described in these proceedings.[15]

Details on the instrumentation used for these observations, along with calibration observations and data reduction procedures, are given in Tyler, et al.[16]

2.2. Launch events

2.2.1. Atlas 5

The first observations were of an Atlas 5-421 carrying a Loral communications satellite and launched on 14 April 2008. The "421" configuration suffix means the payload was enclosed in the Atlas 4-m fairing, two solid-rocket boosters were strapped on to the liquid engine first stage, and a single-engine Centaur upper stage was used (a two-engine Centaur can be used). The Atlas 5 first stage is a Russian-built RD-180 engine, which has two engine bells. The orientation of the Atlas was such that our instruments could see the plumes from the two solid rocket boosters and the two RD-180 bells quite well; that is, during the early part of the flight, our instrument's line-of-sight was nearly normal to a plane containing exhaust from all four bells.

The launch occurred at 1612 EDT, with broken clouds between 3,000 and 5,000 ft. While the countdown and launch were flawless, the vehicle entered clouds shortly after launch, preventing us from observing for longer than a few seconds. The vehicle became visible again after passing through the clouds, and we were able to acquire it, although it was quite a bit further downrange. Incidentally, this particular rocket was lifting the heaviest payload ever carried to orbit by an Atlas 5 and the heaviest commercial satellite ever launched.

2.2.2. STS-124

The orbiter *Discovery* was launched on 31 May 2008, carrying the Japanese "Kibo" laboratory module to the International Space Station. The launch occurred at 1702 EDT, in the first seconds of the launch window. The sky was completely clear in the direction of the shuttle's ascent, allowing us to collect data for several minutes. Unfortunately, that data has not yet been reduced and analyzed.

2.2.3. Delta 2

The final launch we observed was a Delta 2-7920H carrying the Gamma-Ray Large Area Survey Telescope (GLAST). The "7" and "2" in the "7920-H" configuration suffix refer to the types of first and second stages used, and the "9" indicates that nine solid rocket boosters are used. Of these nine, 6 are started on launch along with the main engine. After about a minute, these boosters burn out and are jettisoned, after which the three remaining "air start" boosters are ignited. The main engine is a liquid-fuel Pratt & Whitney RS-27A. The "H" in the configuration suffix is for "Heavy" and indicates that the larger of two possible solid boosters sizes are used. The launch occurred at 1205 EDT on 11 June 2008. The weather was partly cloudy, and in an unfortunate bit of timing, a rather large cumulous cloud took position just over the pad during the launch. This meant that again, we only had a very limited time to acquire data before the launch vehicle entered the cloud; further, because the vehicle began a turn directly away from the site almost immediately, the same cloud obscured our line-of-sight again, and we did not acquire the Delta until shortly before ground booster separation. Finally, variable thin, high cirrus continued to obscure our observations.

3. IMAGE RESULTS

3.1. Multi-spectral Atlas 5 images

Stokes 0 images from the Andor and the SSIP are shown in Fig. 1. In the Andor image (left), the flow from the two RD-180 engine bells is clearly resolved, unlike in the SSIP Stokes 0 image (right). Note also the clearly discernable space between the engine bells and the start of "afterburning," where uncombusted fuel begins to burn in the ambient air, in the Andor image. In the SSIP Stokes 0 image, however, a feature is visibly that appears to be either flow mixing between the booster and main engine plumes or a cross-plume shock wave (a "Mach diamond").

Clearly, simultaneous multi-spectral observations are valuable tools for understanding rocket plumes. Over a wavelength range of less than 120 nm, very distinct phenomena are observed. Our results should motivate simultaneous launch observations with a wide variety of sensors, spanning spectra from the near-ultraviolet to the thermal infrared. Even more phenomena would be revealed by multiple-wavelength laser imaging, extending the basic four-band, multi-spectral data already collected at ISTEF.

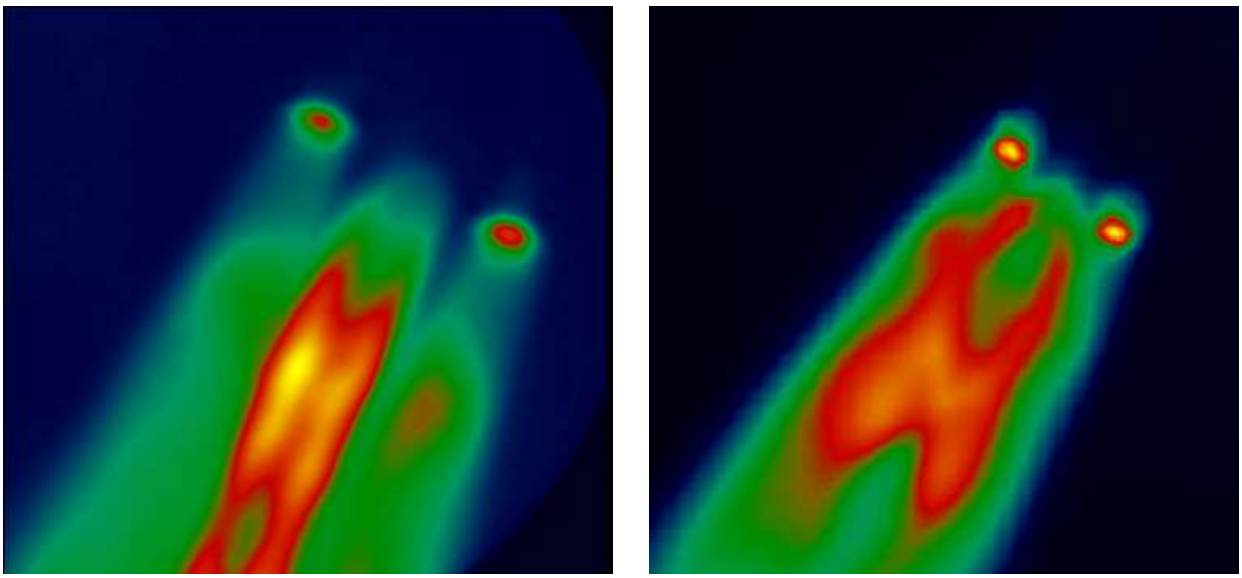

Figure 1. Intensity images of the Atlas 5-421 plumes at 750 nm (left) and 632 nm (right). The images were acquired by two different cameras less than a second apart.

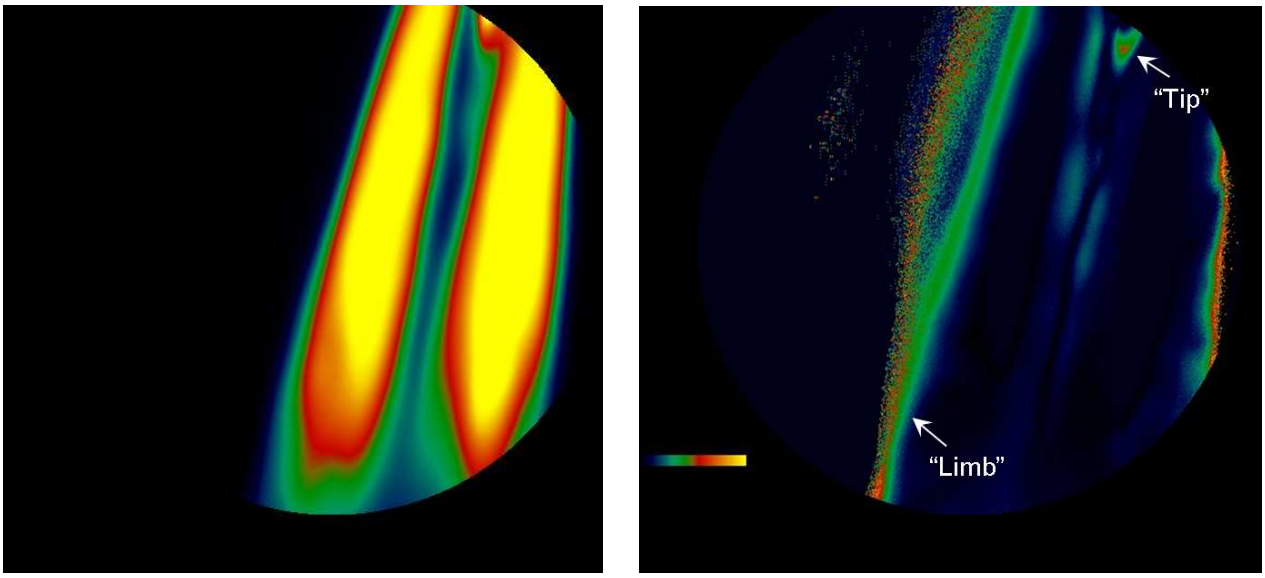

Figure 2. SSIP Stokes 0 (left) and DoLP (right) images of the Atlas 5-421 plumes. Note the polarization color scale in the DoLP image.

3.2. Polarization Atlas 5 and Delta 2 images

In this section, we present linear and circular polarization plume images. We also present evidence the polarization signals are genuine and not the result of misregistration. In subsequent work, we will present a more detailed analysis of polarization in the plumes.

3.2.1. Linear polarization in plume and engine bells

In Fig. 2, we show Stokes 0 (left) and degree of linear polarization (DoLP; right) images of the Atlas 5 plumes. The very innermost part of the solid rocket plumes are saturated; since all four focal plane regions are saturated here, the data reduction yields zero polarization.

Where the image is not saturated, the DoLP is rather low except a.) near the "limbs" of the solid booster plumes and b.) near the bottom of the afterburning part ("tip") of the main engine plume, where DoLP is in the range of 30-60%. The tip of the main engine plume is in the upper right part of the image. Our preliminary assessment of this result is that Rayleigh scattering is the dominant cause of the linear polarization.

To see this, consider that in our proposed Rayleigh scattering scenario, thermal (unpolarized) light would travel from afterburning sources in the plume's interior either

1. along a path directly to the camera (without scattering),
2. along a path in the plane of the image toward the limbs of the plume (or the tip of the main engine plume), where it is scattered out of the plane and then to the camera, or
3. on a path in some plane with surface normal at an arbitrary angle neither in nor normal to the image plane.

If the light were to travel along the second path (in the plane of the image from the plume interior toward the limbs or tip), being scattered at some point through a right angle toward the camera, the resulting light would be linearly polarized. The polarization angle would be in the plane of the image and normal to the direction of propagation from the source to the scatterer. The scattered light is polarized because although randomly-polarized light (that is, unpolarized light) is incident on the scatterer, only light polarized in the image plane will scatter toward the camera; this is, light with a polarization vector pointing toward the camera will never scatter toward the camera.

If the scattering event were to occur before the light reached the limbs or tip, light scattered toward the camera would be "swamped" by unscattered light traveling to the camera without scattering. The much brighter unscattered light would remain unpolarized. Near the limbs or tip, scattered (linearly polarized) light would constitute a much greater fraction of the light propagating toward the camera, producing the results we observe.

Note if light does not travel to the scatterer in the plane of the image, it would be scattered toward the camera through an angle less than 90 degrees. Rayleigh scattering would dictate a much lower DoLP, again consistent with the observation. Also, note that if light does travel in the plane of the image toward the limbs of plume but along any path other than the most direct path (roughly normal to the flow direction), the probability of the light being scattered prior to reaching the limb goes dramatically up. Therefore, light scattered from the limb will have a strong tendency to be polarized only along the direction of flight (nearly vertical). Were this not true, the distribution of polarization angles would be uniform, and the observed DoLP would be very low. In our subsequent work, we will present polarization angle imagery, but for now we argue this DoLP image is consistent with the dominant polarization phenomenon at the SSIP wavelength being Rayleigh scattering.

Before we present the Delta 2 DoLP image, consider the scale model of the Delta 2-7920 shown in Fig. 3.[18] The three solid-fuel, air-start boosters, with slightly larger engine bells, are placed around the main engine (with its single bell) at 120-degree intervals. Two ground-start boosters are placed between each air-start motor.

In Fig. 4, we show SSIP Stokes 0 (left) and DoLP (right) images of the Delta 2 just after liftoff. Note that with the sun nearly directly overhead, the light scattered from the sky has significant (20-30%) linear polarization. The tops and bottoms of the solid rocket booster casings surrounding the Delta 2 fuselage are just visible in the DoLP image, but for the most part, the light coming from the direction of the boosters has the same polarization

Figure 3. Scale model of a Delta 2 in the 7920 configuration. The three "air-start" solid rocket boosters, with their somewhat larger engine bells, are placed around the main engine at 120-degree intervals. Two "ground-start" boosters are placed in between each air start motor. Image copyright Erick Muñoz 2000-2008; used by permission.

as the sky background. This indicates that with the nearly sun overhead and very little small-angle illumination, light reflected from the rocket doesn't add to the DoLP from the sky. Keep in mind that although the airmass between the rocket and camera is much smaller than the airmass behind the rocket, the amount of light scattering changes only the brightness of the measured light, not the DoLP.

Interestingly, the afterburning part of the main engine plume is much brighter than all other sources, while the main engine bell is dark and the exhaust gas between the engine bell and the start of afterburning is very dim (as seen by the red and blue on the Stokes 0 color scale). In the DoLP image, however, the afterburning part of the main engine plume is nearly invisible with the sky having a much stronger signal. Strongly polarized light from what certainly appear to be three booster engine bells provide a convenient reference for other features. Given the angle at which the booster engine bells are tilted (pointing the exhaust slightly radially outward, away from the launch vehicle) these three features could be caused by sunlight or ambient light reflected from the outside of the engine bells.

The DoLP feature in between the center and right engine bells is consistent with ambient light reflected by the main engine bell, which is some what lower than the booster exhausts. Note the DoLP in this feature is at the same level as the diffuse scattering from the booster casings. Also, gas between the bell and the start of afterburning (as seen in the Stokes 0 image) has significant DoLP, somewhat stronger than the sky, while the visible part of the afterburning is very dark in DoLP. In our experience observing Delta 2 engines with fewer solid rocket boosters, the afterburning part of the main engine plume is substantially larger than what is visible in the Stokes 0 image of Fig. 4. Given the optical thickness of the booster plumes, this means much of the main engine plume is obscured, including the "limbs" and "tip" of the plume, where we would expect to see significant DoLP from Rayleigh scattering. In the two visible limbs of the *booster* plume region, we do indeed see linear polarization, and at about the same level (30%, greater than the sky DoLP) as with the Atlas.

We present our final linear polarization image pair in Fig. 5. The left image is an SSIP Stokes 0 image of the Delta 2 launch vehicle as it heads downrange from the site. The right image is the corresponding Stokes 1 image. Unfortunately, the Stokes 2 image had too many saturation events to calculate a useable DoLP image; we suspect these errors originate in faulty registration of noise and stray light in the data. The ground-start boosters have separated, and the air-start boosters are running. At this point in the flight, the main engine plume is unobscured due to the wider separation of the air-start engines. Although the main and booster plumes are indistinguishable in the Stokes 0 image, they can clearly be resolved in Stokes 1.

From the difference in brightness between the left and right sides of the Stokes 0 plume, it's likely the launch vehicle is rotated around its longitudinal axis so that one of two air-start boosters that can be seen by the camera is closer than the other. The difference in orientation between the two boosters produces both a significant difference in both Stokes 0 and Stokes 1 brightness.

We hypothesize the strong linear polarization in the main engine plume and the part of the right-hand booster plume near the engine is a manifestation of small-angle Mie scattering[19] from aluminum soot or similar large, asymmetric particles in the exhaust. Put another way, it is possible we are seeing light from inside or near the engine bell scattering through a relatively small angle to the camera, now looking at the launch vehicle from almost directly behind. The soot or other particles could easily be given a preferential orientation by the flow, inducing polarization effects.

Because the left-hand booster is rotated around the launch vehicle and thus farther from the camera, the polarized light from the limb of that plume is scattered through a larger angle to get to the camera. The DoLP signature from the limb of the left engine plume is again consistent with Rayleigh scattering, with the DoLP level in good agreement with that seen in the two previous examples. The same argument would hold for the part of the right-hand booster plume limb at some distance from the engine bell, where the scattering angle is again large.

Finally, note that at this point in the flight, the Delta 2 is above most of the atmosphere. Since Stokes vectors add, sky polarization increases the the observed polarization from the plume according to

$$D_L(x,y) \;=\; \frac{\sqrt{[S_{1p}(x,y)+S_{1b}(x,y)]^2+[S_{2p}(x,y)+S_{2b}(x,y)]^2}}{S_{0p}(x,y)+S_{0b}(x,y)}, \tag{1}$$

where the p and b subscripts indicate light from the plume and the sky background, respectively. With full angle data and sky background that can plausibly be associated with parts of the plume field under study, the actual (lower) plume polarization can be algebraically estimated. Figure 5, with its variable sky polarization, would be difficult to use in this manner.

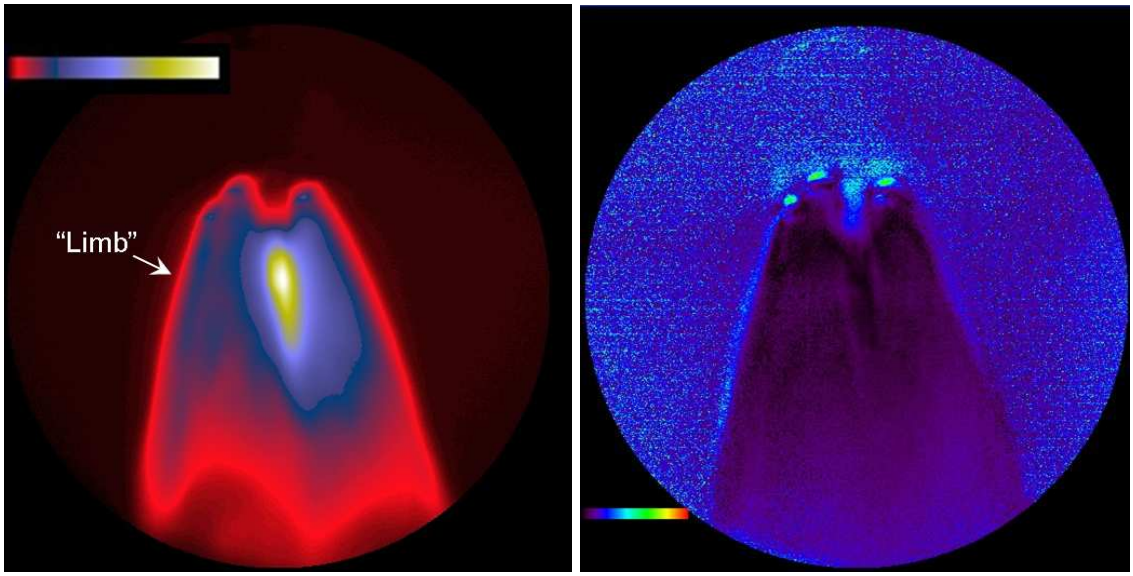

Figure 4. SSIP Stokes 0 (left) and DoLP (right) images of the Delta 2-7920 after launch. Note the polarization color scale in the DoLP image.

3.2.2. False polarization signals and misregistration

As discussed in Tyler, et al.,[16] the four SSIP images must be registered prior to processing. Registration errors will result in false differences in pixel energy between images, causing false polarization signals. This is a rather common source of error in DoAP imaging polarimetry. Because the polarization seen in the plume limbs occurs in reasonably straight lines, the possibility of registration error should be considered. Here are convincing reasons the signals are not the results of misregistration.

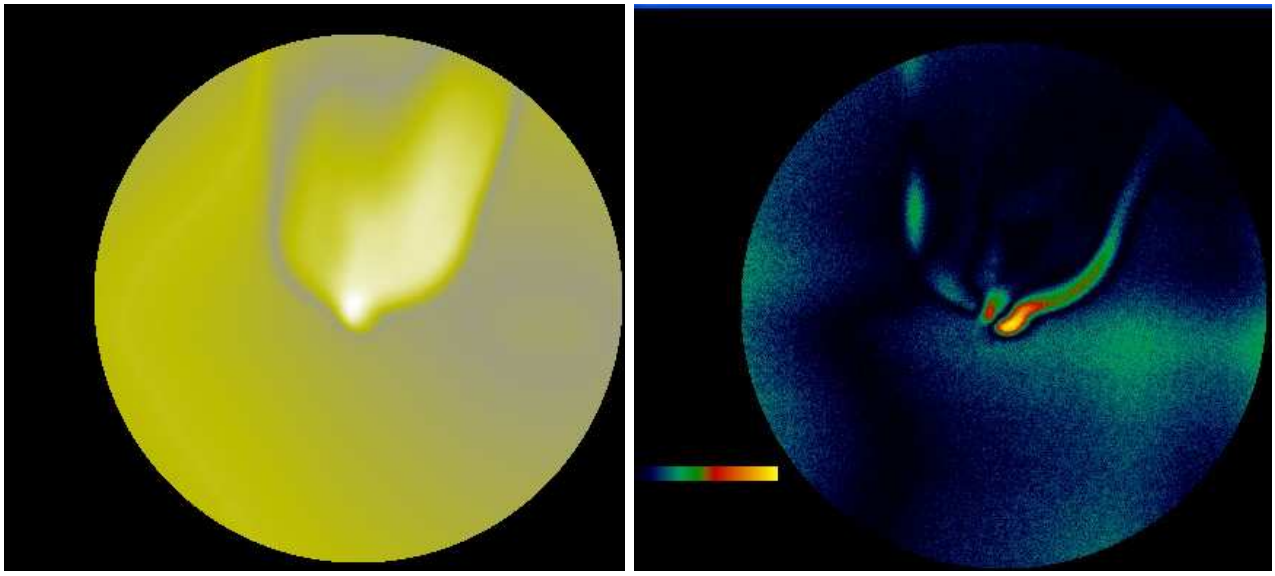

Figure 5. SSIP Stokes 0 (left) and Stokes 1 (right) images of the Delta 2-7920 after ground-start booster separation.

First, it's very unlikely the registration errors required to produce the observed results would occur along an axis exactly normal to the plume limbs; it's even more unlikely that this would occur in multiple images, as would be required to see the limb polarization effect in both Figs. 2 and 4. Second, given the brightness of the main engine plume in the Stokes 0 image in Fig. 4, misregistration would surely cause a false polarization signal in the associated DoLP image; instead, we see near zero DoLP. Finally, the form of polarization signals in DoLP images is duplicated in the corresponding Stokes 0 images: For example, the shape of the DoLP signal seen in the RH image of Fig. 2 main engine plume "tip" is very similar to the main engine plume tip in the LH image. Also, the possible "Mach diamond" or flow-mixing features seen in the RH image of Fig. 1 are present as diffuse polarization features in the LH image in Fig. 6 (note the region inside the white circle).

3.2.3. Circular polarization in Atlas 5 plume

In the Atlas 5 plume, we also observed strong circular polarization, as shown in the Stokes 3 (RH) image in Fig. 6. Note the Stokes 3 image in Fig. 6 and the DoLP image in Fig. 2 are complementary; that is, DoLP is relatively large in the plume limbs, while CP is relatively large in the plume interior.

Plasma electromagnetic field phenomena are complicated, especially in turbulent plasmas. Solid rocket boosters generate plasma in abundance due to the low ionization potentials of alkali metal contaminants in solid rocket fuel; a practical consequence is that launch vehicle telemetry must be relayed to ground stations via satellite rather than broadcast line-of-sight back through the exhaust plume.[20] It is well-known that if the plume plasma interacts with a magnetic field, birefringence can occur, resulting in such CP-producing phenomena as Faraday rotation or the Cotton-Mouton (or "Voigt") effect.[21]

One possible source of the required magnetic field is a velocity sheer between the ionized electrons and their ionic counterparts or between different ionic species in the plume, such as Al^{+} and Cl^{-}. Depending on the evolution of the plume density with distance from the engine and the stagnation of the flow field, such differential velocities could produce an effective current flowing down the plume, creating magnetic field lines around the plume. The relatively high Stokes 3 in the engine bells is consistent with previous numerical studies[20] showing the largest mole fraction of ionized species at the throat of the bell. In on-going work, we are exploring the likelihood of various causal phenomena for both circular and linear observed polarization.

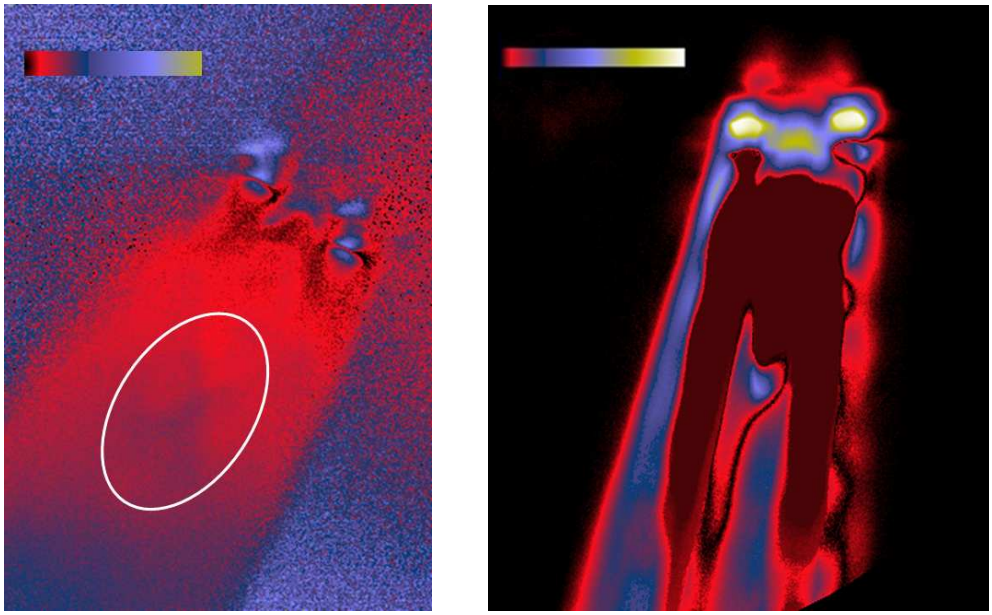

Figure 6. SSIP DoLP (left) and Stokes 3 (right) images of the Atlas 5. The left image corresponds to the Stokes 0 image shown on the right side of Fig. 1. The circle in the left image encloses DoLP features very similar in structure to the Mach diamond / flow-mixing feature seen in the Stokes 0 image.

4. SUMMARY AND CONCLUSIONS

We have presented the first high spatial resolution, passively-illuminated polarimetric images of boosting rocket exhaust plumes. Our results showed significant linear and circular polarization, and the ability to resolve these signals into images allowed us to make some preliminary arguments as to their origin. The polarization observed in our data is consistent with both Rayleigh and Mie scattering (linear) and interaction with plume plasma-generated magnetic fields (circular). We also presented the first two-color, narrow-band exhaust plume images and noted strong structural differences in the plumes at 633 and 750 nm wavelengths. We argue that the understanding of rocket plume phenomenology can be significantly advanced, and robust scaling law and *ab initio* numerical models can be developed and validated, by investing in a broad, multi-sensor program of observations. To our knowledge, prediction of the results shown here are well beyond the capability of existing models. We further argue that hyperspectral imaging over near-IR bands would offer valuable initial insights and provide direction for subsequent observations.

ACKNOWLEDGMENTS

We warmly acknowledge Jason Lehman, Rolf Ahlgreen, and Dan Hand of ISTEF-CSC, without whose professionalism, enthusiasm, and experience this experiment would surely have been much more difficult and much less fruitful. We also acknowledge very productive technical and planning discussions with Richard Tansey, Lockheed Martin ATC. Finally, we gratefully acknowledge funding from the following Lockheed Martin Space Systems Company ATC Internal Research & Development portfolios: 1.) Modeling, Simulation, & Information Sciences, and 2.) Electro-Optics.

REFERENCES

1. A.M. Phenis, M. Virgen, & E. de Leon, "Achromatic instantaneous Stokes imaging polarimeter," in *Novel Optical Systems Design and Optimization VIII*, J. Sasian, R.J. Koshel, & R.C. Juergens, eds., Proc. SPIE **5875**, 587502 (2005)

2. M.R. Descour, C.E. Volin, E.L. Dereniak, T.M. Gleeson, M.F. Hopkins, D.W. Wilson, & P.D. Maker, "Demonstration of a computed tomographic imaging spectrometer using a computer-generated hologram disperser," Appl. Opt. **36**, pp. 3694-3698 (1997)
3. A.A. Alexeenko, N.E. Gimelshein, D.A. Levin, R.J. Collins, R.M. Rao, G.V. Candler, S.F. Gimelshein, J.S. Hong, & T. Schilling, "Modeling of flow and radiation in the Atlas plume," J. Thermophysics & Heat Transfer **16**, 1, pp. 50-57 (2002)
4. P. Barton, B. Pierce, N. Freeman, A.B. Tietjen, J. Emery, D. Dawson, J. Wendt, R. Moyers, R. Hiers, & M. Lovern, "Atlas spectral imagery data and mechanisms," AIAA Paper 2001-1121 (2001)
5. G.V. Candler, R.M. Rao, K. Sinha, D.A Levin, "Numerical simulations of Altas II rocket plumes," AIAA Paper 2001-0354 (2001)
6. R.M. Rao, K. Sinha, G.V. Candler, M.J. Wright, & D.A. Levin, "Numerical simulations of Altas II rocket motor plumes," AIAA Paper 99-2258 (1999)
7. J.S. Hong, D.A. Levin, R.J. Collins, J. Emery, & A.B. Tietjen, "Comparison of Atlas ground-based plume imagery with chemically-reacting flow," AIAA Paper 97-2537 (1997)
8. A.B. Tietjen, J. Emery, & J. Wendt, "High-resolution mid-IR measurements of Atlas in boost phase," Proc. IRIS Specialty Group on Targets, Background, and Discrimination **1** (1996)
9. R.A. Reed, S.A. Fulkerson, C.J. Fisher, B.W. Hartsfield, D.W. Mackowski, P. Markarian, & J.S. Stryjewski, "Enhanced LWIR soot emission from agglomerates," Proc. JANNAF Exhaust Plume Technology Mtg. (2003; Request this document from AEDC/DOS, Arnold AFS, TN 37389)
10. J.S. Stryjewski, B. Griffis, A. Grunke, J. Salg, B.E. Pierce, P. Poirier, & M. Lovern, "Laser backscatter from liquid propellent rocket plumes: Theory and experiment," Proc. 11th Joint AIAA/BMDO Technology Conference (2002; Request this document from SPAWAR SYSCEN San Diego, Code D853)
11. J.S. Stryjewski, "Soot mass loading and particle size effects on laser backscatter from rocket plumes," AIAA 2001-0356 (2001)
12. J.S. Stryjewski, B. Griffis, A. Grunke, J. Salg, & R. Ahlgreen, "Laser backscatter from liquid propellant rocket plumes: Effect of soot and unburned fuel," Proc. 10th Joint AIAA/BMDO Technology Conference (2001; Request this document from SPAWAR SYSCEN San Diego, Code D853)
13. A.C. Goldberg & A.B. Tietjen, "Observation of the launch of an Atlas 5 EELV with a dual-band QWIP focal plane array," in *Infrared Spaceborne Remote Sensing XI*, M. Strojnik, ed., Proc. SPIE **5152**, pp. 100-144 (2003)
14. , E.J. Beiting & R.A. Klingberg, "K-2 Titan IV stratospheric plume disperion," Aerospace Report TR-97(1306)-1, The Aerospace Corporation, El Segundo, CA (1997)
15. J.D. Mudge, M. Virgen, & P. Dean, "Near-infrared simultaneous Stokes imaging polarimeter," in *Polarization Science and Remote Sensing IV*, J.A. Shaw & J.S. Tyo, eds., Proc. SPIE 7461, 74610L (2009)
16. D.W. Tyler, A.M. Phenis, A.B. Tietjen, M. Virgen, J.D. Mudge, J.S. Stryjewski, & J.A. Dank, "First passive, high-resolution polarimetric images of boosting rocket plumes," in *Polarization Science and Remote Sensing IV*, J.A. Shaw & J.S. Tyo, eds., Proc. SPIE 7461, 74610J (2009)
17. B. Lucas & T. Kanade, "An image registration technique with an application to stereo vision," in Proceedings of the International Joint Conference on Artificial Intelligence, pp. 674-679 (1981)
18. *http://www.ericksmodels.com/gallery/delta2/delta2.html*
19. S.M. Oliver, W.K. McGregor, R.A. Reed, & J.A. Drakes, "Analysis of the AlCl absorption feature and searchlight emission effect observed in solid-propellant rocket plumes," AEDC-TR-92-12, Arnold Engineering Development Center (1992)
20. R. H. C. Lee, I. Chang, & G. E. Steward, "Studies of plasma properties in rocket plumes," SD-TR-82-44, Air Force Systems Command, Space Division (1982)
21. K. Muroo, M. Namikawa, & Y. Takubo, "High-sensitivity detection of magnetically-induced birefringence," Meas. Sci. Tech. **11**, pp. 32-37 (2000)